Research Article | Vol. 33, No. 19 / 22 Sep 2025 / Optics Express 40661
Optics EXPRESS

Algorithm for interferometric phase signal demodulation using a 3×3 coupler

Xi Chen,[1,2] Yulin Qiu,[1] Weimin Lyu,[1] Zehao Yu,[3,*] Zhaohui Li,[2,4] and Changyuan Yu[1]

[1]Department of Electrical and Electronic Engineering, The Hong Kong Polytechnic University, Hung Hom, Hong Kong SAR, China
[2]The Southern Marine Science and Engineering Guangdong Laboratory (Zhuhai), Zhuhai 519082, China
[3]School of Instrumentation Science and Engineering, Harbin Institute of Technology, Harbin 150001, China
[4]School of Electronics and Information Technology, Sun Yat-sen University, Guangzhou 510275, China
[*]yuzehao@hit.edu.cn

Abstract: Accurate phase demodulation is essential for high-precision interferometric sensing with 3×3 couplers, but conventional methods are often limited by noise sensitivity and channel mismatches. We propose a robust phase demodulation algorithm that combines principal component analysis (PCA) with nonlinear least-squares ellipse fitting (EFA). The algorithm projects measured signals onto a unified two-dimensional subspace using PCA, enhancing noise suppression and ensuring global consistency during phase fitting. By employing trust-region reflective (TRF) optimization for ellipse fitting, the method achieves high stability and accuracy even in challenging scenarios. Experimental results show that, compared to traditional pairwise EFA, the proposed PCA-EFA approach improves mean SNR by 4.26 dB and reduces THD by 3.27% on average. The algorithm also achieves excellent amplitude linearity (R^2 = 99.9908%) and remains robust for phase amplitudes as low as $\frac{\pi}{8}$. These results demonstrate substantial advantages in accuracy, robustness, and noise immunity, making it highly suitable for advanced interferometric sensing applications.

1. Introduction

In recent years, owing to the high sensitivity, interferometric fiber optic sensors have found extensive applications in critical areas such as hydroacoustic detection, vital signs monitoring, and seismic monitoring [1–4]. These sensors measure environmental parameters through optical interference phenomena; however, their implementations vary widely between different architectures. For instance, interferometric sensors based on Michelson and Mach-Zehnder configurations detect micro-vibrations by extracting phase variations from dynamic interference fringe patterns [5]. Furthermore, Fabry–Pérot interferometric sensors, which exploit multibeam interference within an optical cavity, have been developed for high-resolution detection of small changes in optical path length [6]. Similarly, distributed sensing systems such as phase-sensitive optical time-domain reflectometry (ϕ-OTDR) achieve kilometer-scale spatial monitoring by analyzing phase changes in coherent Rayleigh backscattering [7–9]. Despite these operational differences, all systems rely on precise interferometric signal demodulation to convert optical disturbances into measurable signals.

Effective demodulation of interferometric phase signals is crucial for sensing applications, with primary methods including the Hilbert transform, phase generated carrier (PGC) approach, and 3×3 coupler demodulation [10–15]. Although the Hilbert transform and PGC demodulation are widely used in different types of interferometric systems, their limitations, such as high sensitivity to noise for the Hilbert transform, and complex modulation/demodulation processes as well as susceptibility to high-frequency noise for PGC, have spurred the development of 3×3 coupler-based demodulation algorithms for dynamic and distributed sensing.

#573873 https://doi.org/10.1364/OE.573873
Journal © 2025 Received 18 Jul 2025; revised 21 Aug 2025; accepted 31 Aug 2025; published 16 Sep 2025

Optics EXPRESS

Compared with these conventional methods, 3×3 coupler demodulation leverages the intrinsic phase-shifted outputs of the coupler to enable real-time phase recovery and has become a focus of recent research. However, existing 3×3 demodulation schemes still face significant challenges. Traditional two-dimensional ellipse fitting methods, which rely on pairwise channel combinations, are vulnerable to noise and manufacturing variations. These methods cannot fully correct all errors present in the signals and often lead to inconsistent phase results among different two-channel combinations [16–21]. To address these issues, advanced algorithms such as three-dimensional ellipsoid fitting have been proposed [22], which theoretically provide a more robust model by capturing the full relationship among all three channels. However, these methods require the estimation of 13 parameters, including ten for the ellipsoid and three for the fitting plane, resulting in significant computational complexity and potential numerical instability. In practice, the high dimensionality makes ellipsoid fitting sensitive to outliers and prone to unstable parameter estimation, especially when data are limited or noisy. These factors complicate real-time implementation and reduce overall robustness in practical scenarios, particularly when the signal-to-noise ratio is low or the system exhibits non-idealities.

In contrast, the proposed PCA-EFA algorithm fully utilizes data from all three channels by projecting the inherently three-dimensional signal space onto a unified two-dimensional plane. This global projection ensures consistent and accurate phase demodulation, effectively eliminating the inconsistencies often observed in pairwise channel methods. The reduced dimensionality not only streamlines the computational process and shortens fitting time, but also greatly enhances robustness against noise and outliers compared to conventional advanced 3×3 demodulation algorithms. Furthermore, PCA-EFA supports incremental fitting, enabling real-time adaptation and continuous refinement as system conditions evolve, which is particularly beneficial in practical engineering scenarios. Collectively, these features make PCA-EFA a highly robust and efficient solution for real-time interferometric signal demodulation, delivering superior performance and reliability in dynamic and noisy environments such as fiber optic sensing and distributed monitoring applications.

2. Principle

The proposed PCA-EFA (TRF-based) algorithm provides a robust and efficient approach to interferometric signal demodulation. By fully exploiting the phase-shifting characteristics of the 3×3 coupler, the algorithm combines PCA with the EFA to accurately model coupler parameters and compensate for inherent errors. This methodological approach facilitates precise optical phase demodulation, effectively suppresses noise, and enhances robustness against drifts in the interferometer operating point. The subsequent sections detail the implementation steps of the algorithm.

As shown in Fig. 1, the process begins with acquiring three-channel light intensity signals via a 3×3 coupler. PCA is applied to compute a projection matrix that reduces the data to a two-dimensional subspace, preserving key signal features while suppressing noise. Ellipse fitting is applied to the projected data to extract key geometric parameters. These parameters subsequently correct the signal through normalization, enabling accurate reconstruction of orthogonal components. Finally, the phase is extracted using the ATAN method, followed by phase unwrapping and post-processing to recover a continuous interferometric phase.

According to the interference signal model of the 3×3 coupler, the detector receives three light intensity signals, each of which corresponds to an output channel of the coupler and is described

Optics EXPRESS

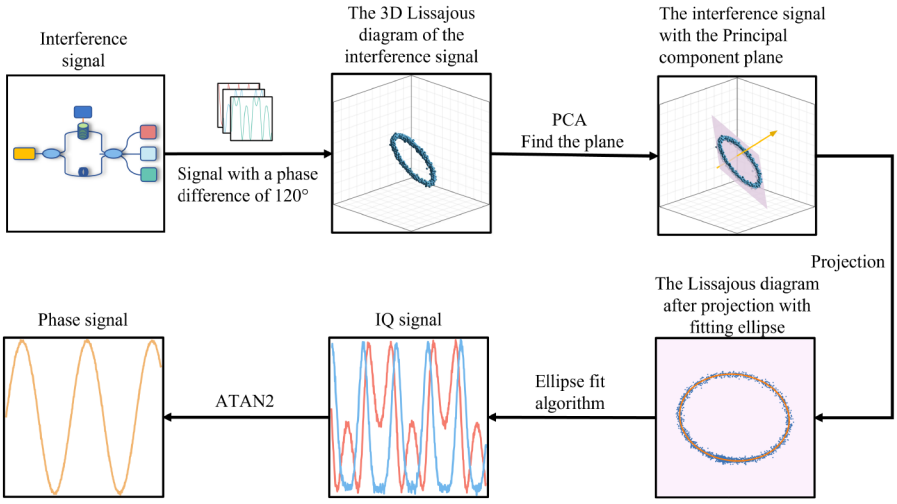

Fig. 1. Flow chart of the PCA-EFA algorithm.

by

$$\begin{aligned} I_1 &= A_1 + B_1 \cos\Big(\varphi(t) + \beta_1\Big), \\ I_2 &= A_2 + B_2 \cos\Big(\varphi(t)\Big), \\ I_3 &= A_3 + B_3 \cos\Big(\varphi(t) - \beta_2\Big), \end{aligned} \tag{1}$$

where the parameters A_i and B_i (with $i = 1, 2, 3$) denote the DC and AC components, respectively, jointly affected by laser intensity noise, coupler splitting ratio, and polarization states. β_1 and β_2 are the phase differences between the interference signals, ideally $\frac{2\pi}{3}$. The interferometer phase signal $\varphi(t)$ is given by

$$\varphi(t) = \frac{2\pi f\, \Delta L}{c}, \tag{2}$$

where f is the light frequency (subject to laser noise), ΔL is the arm length difference (sensitive to vibrations), and c is the speed of light.

2.1. Principal component analysis and projection

The signal model of the 3×3 coupler Eq. (1) shows that the measured data form an elliptical trajectory in three-dimensional space. PCA identifies the principal directions of variation. The light intensity measurements from the three interferometric channels are organized into a matrix X, where each row represents a single observation, as illustrated in Eq. (3).

$$X = \begin{pmatrix} A_1 & A_2 & A_3 \end{pmatrix} + \begin{pmatrix} \cos(\varphi(t_1) + \beta_1) & \cos(\varphi(t_1)) & \cos(\varphi(t_1) - \beta_2) \\ \cos(\varphi(t_2) + \beta_1) & \cos(\varphi(t_2)) & \cos(\varphi(t_2) - \beta_2) \\ \vdots & \vdots & \vdots \\ \cos(\varphi(t_N) + \beta_1) & \cos(\varphi(t_N)) & \cos(\varphi(t_N) - \beta_2) \end{pmatrix} \begin{pmatrix} B_1 \\ B_2 \\ B_3 \end{pmatrix} \tag{3}$$

To prepare the data for PCA, the mean value of each channel is subtracted. This yields the mean-centered matrix X_c, as defined in Eq. (4):

$$X_c = X - \bar{X}, \tag{4}$$

Optics EXPRESS

where $\bar{X}$ denotes the mean value of the data matrix X. Singular value decomposition (SVD) is then performed on the mean-centered matrix X_c as:

$$X_c = U\Sigma V^T, \tag{5}$$

where Σ contains the singular values, and V^T contains the principal directions. The two largest singular values and their corresponding vectors are selected to capture the directions of maximum variance, enabling dimensionality reduction and noise suppression.

The eigenvectors corresponding to the two largest singular values are arranged into a projection matrix V_2 as defined in Eq. (6):

$$V_2 = \begin{pmatrix} B_1\cos(\beta_1) & -B_1\sin(\beta_1) \\ B_2 & 0 \\ B_3\cos(\beta_2) & B_3\sin(\beta_2) \end{pmatrix}. \tag{6}$$

The data matrix X is projected onto the two-dimensional subspace defined by the projection matrix V_2 (Eq. (6)), yielding the projected data X_p as shown in Eq. (7):

$$X_p = XV_2. \tag{7}$$

The $X_p = [x_p, y_p]$ represents the two-dimensional projected signals. The explicit expressions for the projected signals are given by Eq. (8):

$$\begin{aligned} x_p &= B_1^2\cos(\beta_1)\cos\big(\varphi(t)+\beta_1\big) + B_2^2\cos\big(\varphi(t)\big) + B_3^2\cos(\beta_2)\cos\big(\varphi(t)-\beta_2\big) + B_1A_1\cos(\beta_1) \\ &\quad + B_2A_2 + B_3A_3\cos(\beta_2), \\ y_p &= -B_1^2\sin(\beta_1)\cos\big(\varphi(t)+\beta_1\big) + B_3^2\sin(\beta_2)\cos\big(\varphi(t)-\beta_2\big) - B_1A_1\sin(\beta_1) + B_3A_3\sin(\beta_2). \end{aligned} \tag{8}$$

Here, x_p and y_p are the components obtained after projection, linear combinations of the original channel signals weighted by the coupler parameters.

Under ideal conditions, where $B_1 = B_2 = B_3$ and $\beta_1 = \beta_2 = \frac{2\pi}{3}$, the two signals (x_p, y_p) form a perfect circle in the two-dimensional plane, representing ideal orthogonal signals. However, in practical scenarios, imperfections such as unequal coupler splitting ratios and noise cause the parameters B_1, B_2, B_3, β_1, and β_2 to deviate from their ideal values. As a result, the projected signals (x_p, y_p) trace out an ellipse rather than a circle. In such cases, ellipse fitting is necessary for subsequent data correction and accurate phase demodulation.

In actual sensing systems, various types of system noise, including laser intensity noise and coherence fading, can affect the measured signals and impair the performance of the EFA algorithm. Laser intensity noise leads to fluctuations in signal amplitude, while coherence fading, which results from random changes in the fiber's birefringence and polarization state, introduces joint amplitude and phase fluctuations that can significantly reduce the orthogonality of the projected signals. In particular, polarization fading, a specific manifestation of coherence fading caused by imperfect alignment or rapid changes in the state of polarization, can further exacerbate amplitude variations. These effects may distort the ideal geometric structure of the data in the principal component space and increase the difficulty of accurate phase demodulation. Nevertheless, as long as the signal remains the dominant component in the principal components and the noise is primarily random, the EFA algorithm can still identify the optimal solution that best compensates for system imperfections.

This projection not only reduces dimensionality but also serves as a denoising step. Based on experimental observations and noise analysis, the measured data can be reasonably modeled as $X = S + N$, where S denotes the underlying signal and N represents additive Gaussian noise as well

Optics EXPRESS

as the aforementioned system noise. After mean-centering and filtering, the data are expressed as $X_f = S_f + N_f$, where S_f and N_f are the filtered signal and noise components, respectively. The matrix X_f is then projected onto the principal directions captured in V_2, yielding $X_p = X_f V_2$. Through this projection, most of the signal energy in S_f is preserved, as it is concentrated along the directions of highest variance. In contrast, the noise N_f, which is distributed more uniformly across all directions, contributes less to the projected subspace. Consequently, the projection step facilitates the suppression of both random and structured system noise, thereby enhancing the quality of the extracted signals and improving the accuracy of subsequent phase demodulation.

2.2. Ellipse fitting and signal correction

Under non-ideal conditions, the projected data points exhibit an elliptical distribution, making ellipse fitting essential for subsequent data correction and accurate phase demodulation. This elliptical pattern can be mathematically represented by the general quadratic equation given in Eq. (9):

$$Ax^2 + Bxy + Cy^2 + Dx + Ey + F = 0. \tag{9}$$

The given set of data points $I_x^{(N)}, I_y^{(N)}$ is fitted using EFA by minimizing the sum of squared algebraic residuals as follows:

$$\min_{A,B,C,D,E,F} \sum_{i=1}^{N} \left(Ax_i^2 + Bx_i y_i + Cy_i^2 + Dx_i + Ey_i + F\right)^2. \tag{10}$$

To solve this problem, the direct least-squares (DLS) fitting method [23] is employed and implemented as follows. First, a design matrix is constructed from the data points (I_x, I_y), with the quadratic terms $(I_x^2, I_x I_y, I_y^2)$ separated from the linear terms $(I_x, I_y, 1)$. Matrix operations are then performed to compute the scatter matrices, and the resulting linear system is solved using a pseudo-inverse for numerical stability. The solution is further refined by performing eigenvalue decomposition on an adjusted matrix, and the eigenvector that satisfies the ellipticity constraint $4AC - B^2 > 0$ is selected, ensuring that the fitted parameters correspond to a valid ellipse.

Thus, the parameters of the algebraic equation are converted into ellipse parameters to further improve fitting accuracy and enable ellipse correction.

The center of the ellipse is given by Eq. (11):

$$x_0 = \frac{2CD - BE}{B^2 - 4AC}, \quad y_0 = \frac{2AE - BD}{B^2 - 4AC}. \tag{11}$$

The lengths of the semi-axes are calculated according to Eq. (12). For clarity, several intermediate variables are introduced as follows:

$$\begin{aligned} \delta &= (A - C)^2 + B^2, \\ \Psi &= AE^2 + CD^2 + BDE - (B^2 + 4AC)F. \end{aligned}$$

Then,

$$\begin{aligned} a &= \sqrt{\frac{2\Psi}{(B^2 - 4AC)\left[(A + C) - \sqrt{\delta}\right]}}, \\ b &= \sqrt{\frac{2\Psi}{(B^2 - 4AC)\left[(A + C) + \sqrt{\delta}\right]}}. \end{aligned} \tag{12}$$

The rotation angle required to align the ellipse with the coordinate axes is given by Eq. (13):

$$\phi = \frac{1}{2} \arctan 2\big(B, A - C\big). \tag{13}$$

Optics EXPRESS

Due to the sensitivity of the algebraic residual to noise, the initial ellipse fitting results are further refined using a nonlinear least-squares approach. Rather than normalizing each data point, the ellipse parameters (x_0, y_0, a, b, ϕ) are directly optimized by minimizing the overall residual. The residual for each data point $(I_x^{(t)}, I_y^{(t)})$ is defined as:

$$\begin{aligned} r_t = &\left[\frac{(I_x^{(t)} - x_0)\cos\phi + (I_y^{(t)} - y_0)\sin\phi}{a}\right]^2 \\ &+ \left[\frac{-(I_x^{(t)} - x_0)\sin\phi + (I_y^{(t)} - y_0)\cos\phi}{b}\right]^2, \end{aligned} \tag{14}$$

where $I_x^{(t)}$ and $I_y^{(t)}$ are the t-th data point coordinates.

The nonlinear least-squares problem is formulated as follows:

$$\min_{x_0, y_0, a, b, \phi} \sum_{i=1}^{N} (r_i - 1)^2. \tag{15}$$

This optimization is solved iteratively using nonlinear least-squares algorithms such as the Gauss-Newton method, the Levenberg-Marquardt (LM) algorithm, or the Trust Region Reflective (TRF) algorithm. These methods provide accurate estimates of the ellipse parameters by minimizing the total residual error.

Once the refined ellipse parameters (x_0, y_0, a, b, ϕ) have been determined, the original signal is corrected accordingly. This correction is achieved by scaling, translating, and rotating the signal, thereby yielding two orthogonal signals, which are subsequently utilized for phase demodulation.

$$\begin{aligned} I_x'^{(t)} &= \frac{(I_x^{(t)} - x_0)\cos\phi + (I_y^{(t)} - y_0)\sin\phi}{a}, \\ I_y'^{(t)} &= \frac{-(I_x^{(t)} - x_0)\sin\phi + (I_y^{(t)} - y_0)\cos\phi}{b}, \end{aligned} \tag{16}$$

which maps points initially lying on the ellipse onto a unit circle. The corrected orthogonal signals will be used for subsequent phase demodulation.

2.3. Phase demodulation

The phase $\varphi(t)$ is calculated from the two orthogonal signals using the arctan 2 function. This method yields a full-range angular output and eliminates quadrant ambiguity:

$$\varphi(t) = \arctan 2\left(I_y'^{(t)}, I_x'^{(t)}\right), \tag{17}$$

where $I_y'^{(t)}$ and $I_x'^{(t)}$ are the corrected orthogonal signals. This approach ensures precise phase demodulation by directly mapping the geometric relationship between the two signals to the phase angle. The resulting phase is then unwrapped to obtain a continuous phase signal.

3. Simulation

In this section, the performance of the proposed PCA-EFA algorithm is systematically evaluated against that of the traditional pairwise EFA method. To ensure a fair comparison, the same TRF nonlinear least-squares ellipse fitting is employed for both algorithms, thereby isolating the impact of the signal processing structure–namely, PCA-based projection versus conventional pairwise channel processing–on noise suppression and phase recovery accuracy. To comprehensively

Optics EXPRESS

assess the effectiveness and robustness of PCA-EFA, numerical simulations are conducted across various noise levels and coupler parameter settings. For each configuration, 50 independent trials are performed to ensure statistical reliability. The resulting SNRs are summarized using box plots to provide a clear and quantitative comparison of algorithm performance under diverse conditions.

3.1. Comparison of TRF nonlinear least-squares ellipse fitting and DLS ellipse fitting

The first simulation compares the direct TRF and DLS ellipse fitting methods for phase demodulation using PCA-projected data. The TRF nonlinear least-squares ellipse fitting consistently outperforms the DLS method, especially under high noise levels and low phase amplitudes. As shown in Fig. 2, the DLS method often fails for phase amplitudes below $\frac{\pi}{4}$, whereas the TRF method maintains robustness.

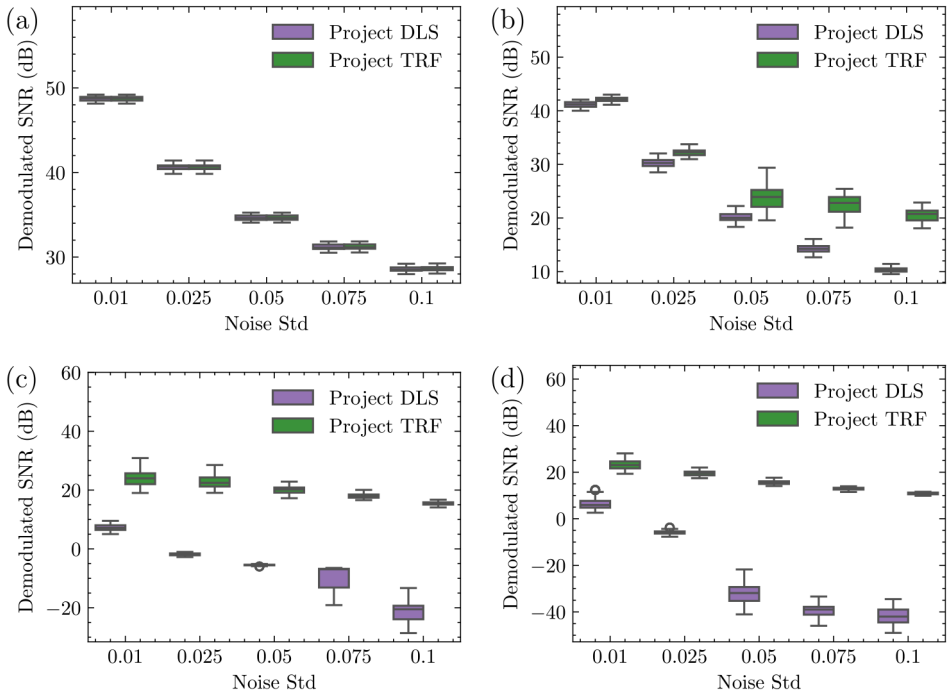

Fig. 2. Demodulated SNR versus noise standard deviation for different phase amplitudes using PCA-EFA (TRF-based) and PCA-EFA (DLS-based) algorithms. Box plots depict the distribution of SNR values: the central line indicates the median, the box edges represent the first and third quartiles, and the whiskers extend to the most extreme data points within 1.5 times the interquartile range. Outliers beyond this range are shown as individual points. (a) Phase amplitude = π; (b) Phase amplitude = $\frac{\pi}{2}$; (c) Phase amplitude = $\frac{\pi}{4}$; (d) Phase amplitude = $\frac{\pi}{8}$.

The results, shown in Fig. 3, demonstrate that the PCA-EFA (TRF-based) method achieves significantly higher demodulated SNR than the pairwise EFA (TRF-based), particularly at low phase amplitudes and higher noise levels. Across all data, the PCA-EFA (TRF-based) method yields a mean SNR of 25.38 dB, compared to 18.97 dB for the pairwise EFA (TRF-based), representing an average improvement of 6.41 dB. For phase amplitudes less than $\frac{\pi}{2}$, the average improvement reaches 7.62 dB. These results confirm that the PCA-based projection effectively enhances noise suppression and signal fidelity in phase demodulation, providing clear advantages over conventional techniques.

Optics EXPRESS

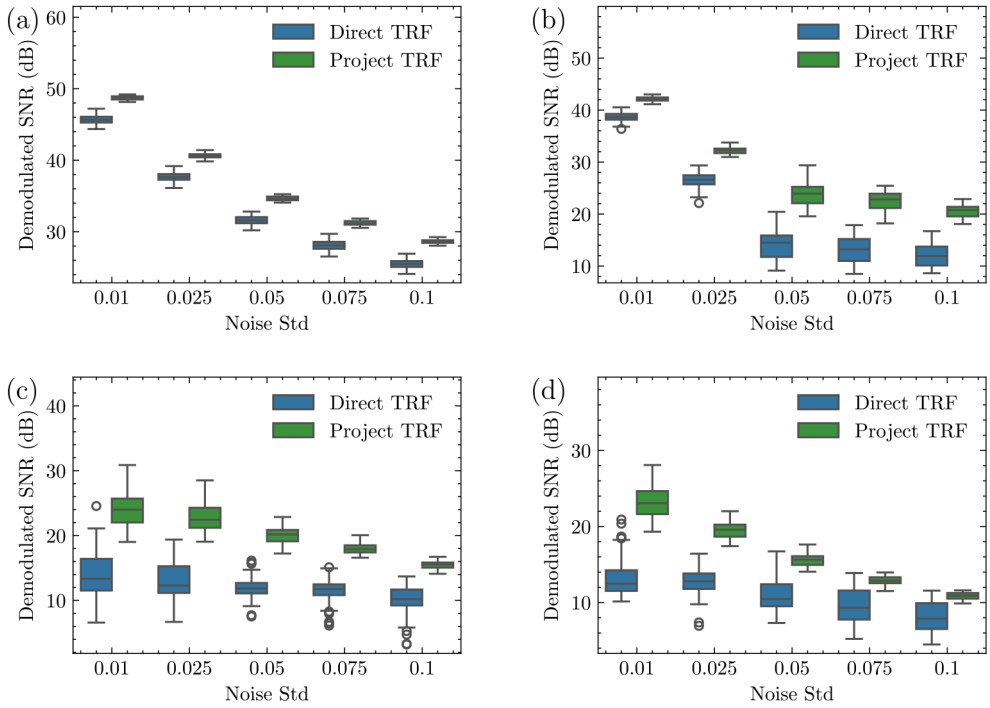

Fig. 3. Comparison of demodulated SNR under different noise standard deviations and signal phase amplitudes using three methods: Direct, Denoise, and Project. (a) Phase amplitude = π; (b) Phase amplitude = $\frac{\pi}{2}$; (c) Phase amplitude = $\frac{\pi}{4}$; (d) Phase amplitude = $\frac{\pi}{8}$.

3.2. Comparison of PCA-based projection and pairwise demodulation

The conventional pairwise EFA demodulation method, which performs ellipse fitting and phase demodulation separately on each pair of channels, is compared with the proposed PCA-EFA (TRF-based) demodulation method, in which PCA is first applied to the three-channel signals prior to ellipse fitting and phase demodulation. In both methods, the same TRF nonlinear least-squares algorithm is employed for ellipse fitting.

The results, shown in Fig. 3, demonstrate that the PCA-EFA (TRF-based) method achieves significantly higher demodulated SNR than the pairwise EFA (TRF-based), particularly at low phase amplitudes and higher noise levels. Specifically, the PCA-EFA (TRF-based) method yields a mean SNR of 24.13 dB, while the pairwise EFA (TRF-based) achieves 19.84 dB, representing an average improvement of 4.29 dB. This confirms that the PCA-based projection enhances noise suppression and signal fidelity in phase demodulation, providing clear advantages over conventional techniques.

3.3. Computational complexity, real-time performance, and adaptivity

The proposed PCA-EFA algorithm consists of two main stages. First PCA is performed using singular value decomposition (SVD) on the incoming $N \times 3$ data matrix to extract the dominant signal features and suppress noise. Next, the effective phase is recovered via ellipse fitting, using either direct least squares (DLS) or the more robust trust region reflective (TRF) fitting algorithm. This process is fully data-driven and operates on streaming measurement data, enabling real-time demodulation without the need for prior offline calibration.

Optics EXPRESS

In terms of engineering implementation, the algorithm demonstrates strong real-time performance. On a standard PC (Intel i7-12700, 16 GB RAM), processing a data block of 10^5 samples (0.1 s at a 1 MHz sampling rate) requires 0.011 s for the PCA step, 0.0057 s for DLS-based fitting, and 0.232 s for TRF-based fitting. The SVD step scales linearly with the number of data points ($O(N)$), and both SVD and TRF are well suited for hardware acceleration. Even the more computationally intensive TRF fitting meets the requirements for real-time processing at typical sensor sampling rates. With further optimization and parallelization, the algorithm is suitable for deployment on embedded platforms such as FPGAs or DSPs, supporting high-speed and resource-constrained applications.

In practical sensing environments, system parameters such as the coupler's ratio may drift slowly due to temperature or other environmental factors. The PCA-EFA algorithm addresses this by estimating parameters directly from the most recent data, requiring only a small data block for accurate fitting. Once parameters are estimated, they can be reused for ongoing demodulation, eliminating the need for frequent retraining. To maintain robustness under changing conditions, the algorithm supports periodic or event-driven parameter updates. Parameters may be recalibrated at set intervals or adaptively updated using a sliding window approach when indicators such as IQ non-orthogonality are detected. This ensures consistent demodulation accuracy and system adaptability in dynamic environments without sacrificing real-time performance.

4. Experiment

In the experimental validation, a Mach-Zehnder interferometer (MZI) was constructed, as shown in Fig. 4 and Fig. 5. A highly coherent distributed feedback (DFB) laser provides the optical source. Its output is split by a 1×2 optical coupler into a sensing arm and a reference arm. In the sensing arm, a piezoelectric transducer (PZT) and approximately one meter of coiled optical fiber are driven by an arbitrary waveform generator (AWG) to introduce controlled phase modulation. The reference arm contains a delay fiber, and the lengths of both arms are carefully matched to increase the free spectral range (FSR) and suppress sensitivity to wavelength drifts, despite inevitable experimental tolerances. The two arms are then fed into a 3×3 optical coupler, whose three outputs are monitored by a photodetector (PD) for signal acquisition and subsequent demodulation.

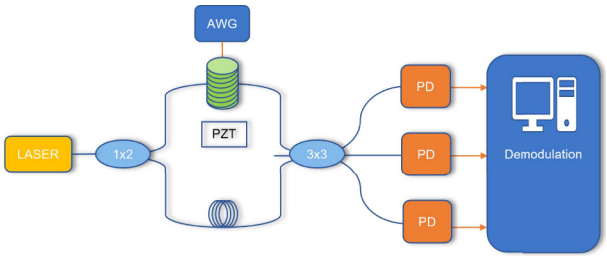

Fig. 4. Experiment setup schematic. AWG: arbitrary waveform generator; PZT: piezoelectric ceramic transducer; PD: photoelectric detector.

4.1. Experimental validation and demodulation comparison

In this section, we analyze and experimentally compare the performance of the PCA-EFA (TRF-based) algorithm and the traditional pairwise EFA(DLS-based). The comparison was conducted using the previously described system with a sampling rate of 200,000 Sa/s and an AWG operating at 5,000 Hz. For the acquired original data, the SNR of the three channels was measured as follows: CH1 SNR: 25.73 dB, CH2 SNR: 26.75 dB, and CH3 SNR: 20.97 dB. The acquired data was demodulated using both algorithms, and the results are shown in Fig. 6.

Optics EXPRESS

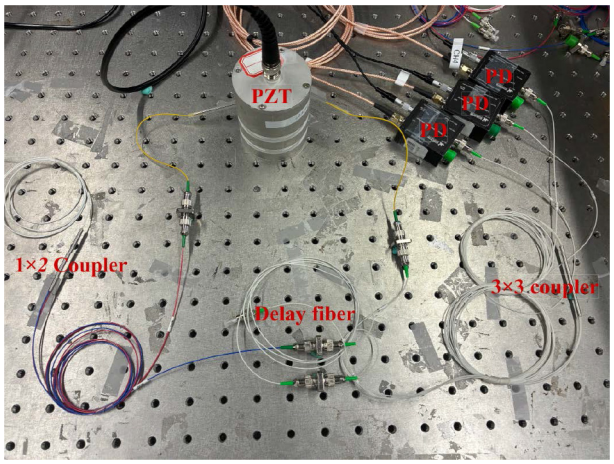

Fig. 5. Experiment setup schematic

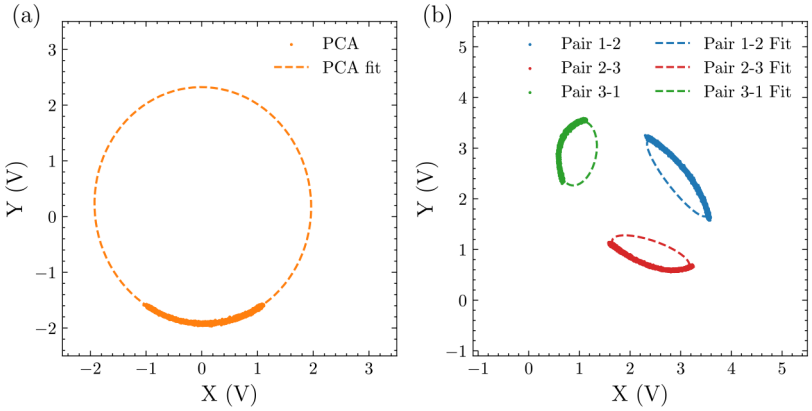

Fig. 6. Comparison of Lissajous figures and fitted ellipses for original signals using different methods. (a) Lissajous figure and fitted ellipse of the signal after PCA. (b) Lissajous figure and fitted ellipse of the original three-channel signal.

Figure 6 illustrates the outcomes of PCA-EFA and traditional EFA analyses on the raw data. Figure 6(a) presents the distribution of data projected by PCA alongside the corresponding TRF-fitted ellipse, highlighting the principal components. Figure 6(b) displays ellipses fitted to all pairwise combinations of the three signals from the 3×3 coupler. The observed asymmetry in the Lissajous figures reflects the influence of manufacturing imperfections, which exposes the limitations of traditional pairwise fitting methods. In the traditional pairwise EFA approach, Lissajous figures are constructed by directly pairing two channels, resulting in ellipses whose aspect ratio and orientation are dictated by the physical properties of the coupler and may be highly eccentric or tilted. When only a small segment of a circular arc is available, the geometric ambiguity becomes much more pronounced. In this scenario, it is generally impossible to impose additional regularization constraints during ellipse fitting without violating the underlying physics of the system. As a result, ellipse fitting in the traditional framework is much more prone to instability, multiple solutions, and numerical deviation, particularly when the signal coverage is limited or the SNR is low.

Optics EXPRESS

A crucial advantage of the PCA-EFA algorithm is its ability to introduce effective regularization during ellipse fitting, and the underlying reason for this capability lies in the geometric properties of the signal after PCA transformation. Specifically, PCA projects the original multichannel data onto an optimal two-dimensional subspace, where, under ideal conditions, the Lissajous figure corresponding to the modulated phase forms a perfect circle. Even in the presence of system non-idealities, the PCA-transformed data typically maintain a nearly circular and symmetric distribution. This circular (or near-circular) structure is fundamentally important for regularization: when the data points are distributed along a circle, the geometric parameters of the fitted shape, such as center, radius, and orientation, are naturally well constrained. In such a case, it becomes possible and meaningful to apply regularization strategies during ellipse fitting, for example, by penalizing deviations from circularity or enforcing orthogonality in the fitted axes. These constraints help stabilize the fitting process, especially in challenging scenarios where only a short arc of the Lissajous figure is observed, and effectively suppress ambiguous or extreme solutions that could otherwise arise from ill-posed fitting problems. Ellipse correction is performed using the TRF nonlinear least-squares fitting algorithm, as shown in Fig. 7(a), where the PCA-EFA algorithm is illustrated. In this approach, the interfering signal is projected onto the principal component plane and corrected using TRF-fitted ellipse parameters, resulting in data points that are nearly aligned with the unit circle. In contrast, Fig. 7(b) presents the traditional pairwise EFA (DLS-based) method, in which pairwise fitting and correction are applied using DLS-fitted parameters for each channel pair.

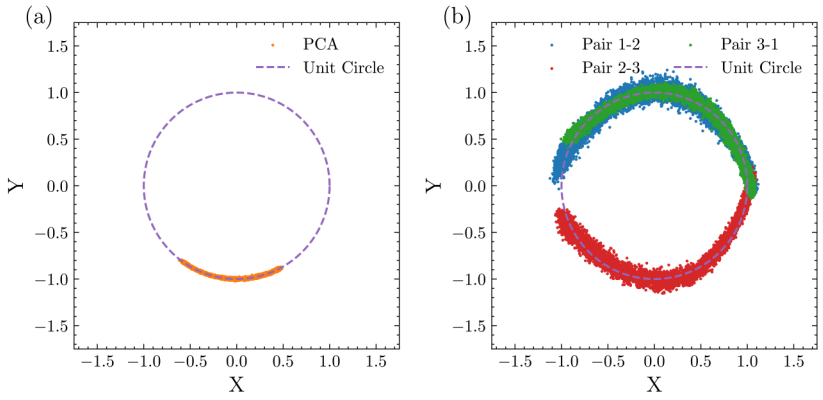

Fig. 7. Corrected Lissajous figures obtained by different methods. (a) Corrected Lissajous figure of PCA-EFA result. (b) Corrected Lissajous figure of pairwise EFA (DLS-based) result.

The comparison of demodulated interferometric phase signals between the PCA-EFA and the traditional pairwise EFA (DLS-based) methods is shown in Fig. 8(a), presenting the complete phase signal, while Fig. 8(b) provides a zoomed view for greater clarity. Only the PCA-EFA algorithm yields successful phase demodulation. The other three demodulated signals exhibit severe amplitude distortion. Although their SNR values, calculated via spectral methods, are not significantly lower, the demodulated results do not match the original phase modulation amplitudes, indicating demodulation failure.

Figure 9 and Table 1 show the THD and demodulated SNR of the traditional pairwise EFA(DLS-based) for each channel pair with those of the proposed PCA-EFA (TRF-based) method. The PCA-EFA achieves the lowest THD (0.16%) and highest SNR (27.09 dB), outperforming all channel pairs. Note that SNR is computed in the frequency domain, where amplitude distortions are not treated as noise. Despite this, the substantial THD reduction and SNR

Optics EXPRESS

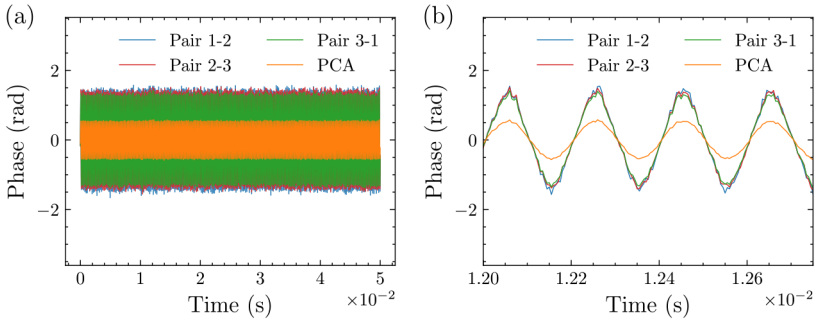

Fig. 8. Demodulated phase signals obtained by different methods. (a) Overall comparison of demodulated phase signals using different methods. (b) Detail of the demodulated phase signals.

improvement demonstrate the PCA-based method's harmonic suppression and noise robustness over conventional pairwise demodulation.

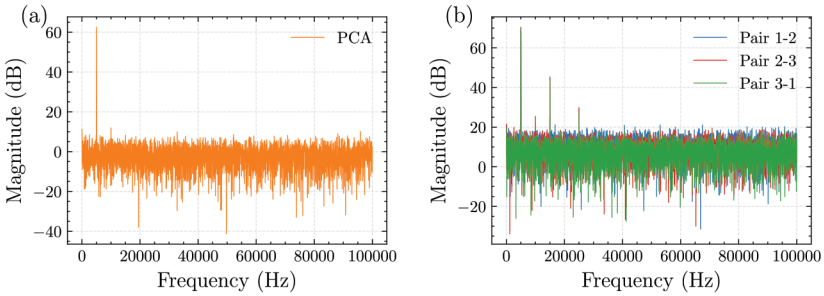

Fig. 9. Comparison of the demodulated signal spectra for two algorithms. (a) Demodulated signal spectrum using the PCA-EFA algorithm. (b) Demodulated signal spectrum using the pairwise EFA (DLS-based) algorithm.

Table 1. THD, Demodulated SNR, and Amplitude comparison for different algorithms.

Method	THD (%)	SNR (dB)	Amplitude (rad)
Pairwise EFA 1-2	5.55	20.95	1.6205
Pairwise EFA 2-3	5.52	21.72	1.5461
Pairwise EFA 3-1	4.85	22.73	1.4276
PCA-EFA (TRF-based)	0.35	27.14	0.5820

4.2. Accuracy and stability evaluation of the PCA-EFA algorithm

To estimate the accuracy and robustness of the proposed PCA-EFA (TRF-based) algorithm, we analyze the linearity of the phase amplitude response and the stability of the PCA projection under varying noise levels and phase-modulation amplitudes. In the experiments, a sinusoidal voltage from 0.5 to 4 V_{pp} (in 0.1 V_{pp} steps) was applied to the PZT, yielding 36 measurements at a sampling rate of 500,000 Sa/s. An optical attenuator was also inserted before the interference signal to test the algorithm further.

Figure 10 shows the principal component planes after PCA projection, with unit normal vectors (blue arrows) and unit circles (green) illustrating normalization for consistent analysis. The mean

Optics EXPRESS

SNRs for channels CH1, CH2, and CH3 are 19.31 dB, 21.29 dB, and 19.25 dB, respectively. The fitted ellipse on the principal component plane is shown in Fig. 11.

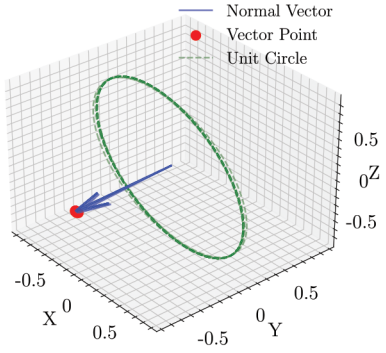

Fig. 10. principal component plane fitted to all 36 ellipses and its normal vector.

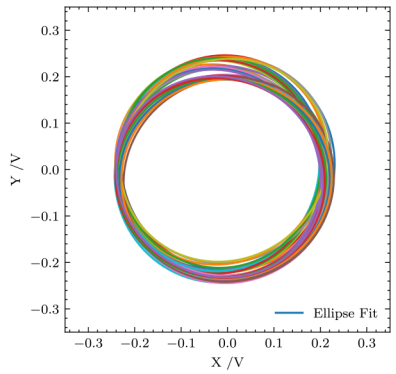

Fig. 11. Ellipse fitting on the principal component plane for 36 experimental trials.

Figure 12 shows that the PCA-EFA (TRF-based) method exhibits an excellent linear relationship between the output amplitude and the driving voltage applied to the PZT. In addition, the proposed algorithm achieves a significantly higher average SNR of 34.12 dB compared to 29.35 dB for the traditional pairwise EFA(DLS-based) method; when the phase amplitude is less than $\frac{\pi}{2}$, the average SNR improvement increases to 6.02 dB. Regarding harmonic distortion, the PCA-EFA method obtains an average THD as low as 0.24%, while the pairwise EFA(DLS-based) yields 3.60%. These results highlight the superior linearity, noise suppression, and harmonic distortion reduction capabilities of the PCA-EFA algorithm.

Figure 13 further verifies the strong amplitude linearity of the PCA-EFA algorithm. Regression analysis reveals that the RMS amplitudes of the demodulated signals maintain an excellent linear correlation with the applied voltage, as evidenced by the fitted straight line (red) and a coefficient of determination (R^2) of 99.9908%. In contrast, the traditional pairwise EFA (DLS-based) method produces unstable demodulated amplitudes when the phase amplitude falls below approximately 1.57 rad, whereas the PCA-EFA algorithm consistently maintains robust linearity across the entire tested range. We also perform a stability experiment. A 2 V sinusoidal driving signal was applied to the PZT in the same experimental setup. Forty-one experiments were performed, with the driving frequency ranging from 1 kHz to 5 kHz in 100 Hz increments. Figure 14 shows the experimental results. The stability of the system is excellent, as indicated by a relative standard deviation (RSD) of only 0.08% for the primary peak amplitude across the measured frequency range.

Optics EXPRESS

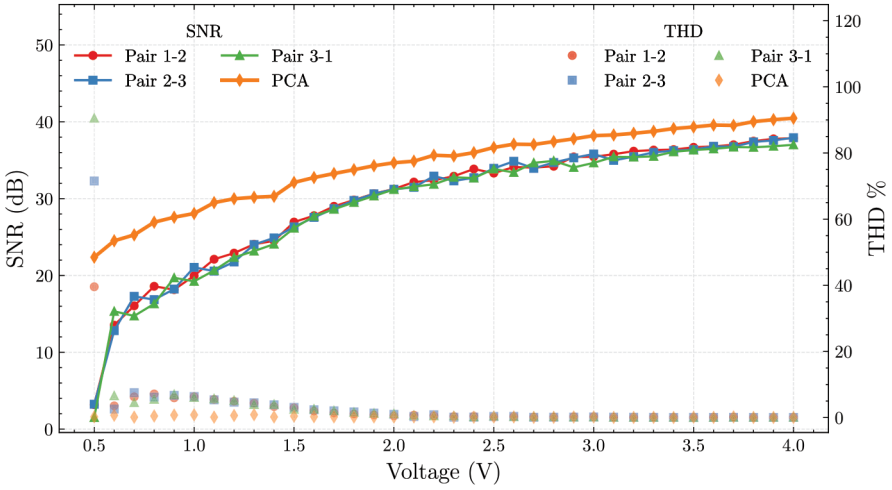

Fig. 12. Comparison of SNR and THD of solution results with different algorithms under a series of PZT sinusoidal driving voltage levels.

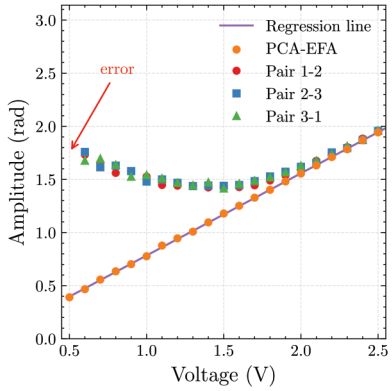

Fig. 13. PCA-EFA demodulated phase amplitudes under sequential PZT sinusoidal driving voltage levels.

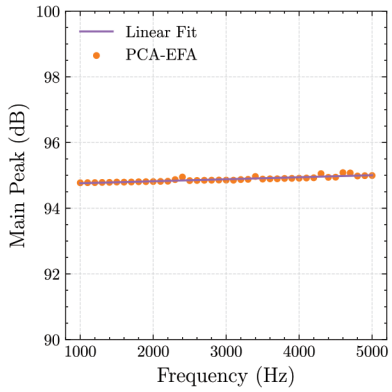

Fig. 14. Primary peak amplitude of signals at different frequencies.

Optics EXPRESS

5. Conclusion

In summary, a robust ellipse fitting algorithm combined with PCA is proposed for accurate phase demodulation of interferometric signals from a 3×3 coupler. The nonlinear least-squares ellipse fitting method is specifically adapted for the elliptical trajectories of three-channel signals, providing stable and precise phase demodulation even under low signal amplitude or strong noise. By introducing PCA, the correlation among the three channels is fully utilized, and the measured data are projected onto a unified two-dimensional subspace, which not only enhances noise suppression but also ensures global consistency and reliability in phase demodulation.

Importantly, compared to the traditional pairwise ellipse fitting algorithm, which can only reliably demodulate phase signals with amplitudes greater than $\frac{\pi}{2}$ due to ellipse fitting errors and amplitude distortion at lower phase shifts, the proposed PCA-EFA (TRF-based) algorithm accurately demodulates phase signals with amplitudes as low as $\frac{\pi}{8}$. This greatly extends the practical applicability of ellipse fitting methods to low-amplitude and high-noise scenarios.

Experimental results demonstrate that, compared with the traditional pairwise ellipse fitting method, the proposed PCA-EFA (TRF-based) algorithm achieves a mean SNR improvement of 4.26 dB and an average reduction of THD by 3.27%, with the maximum THD reduction reaching 5.26%. Furthermore, the amplitude linearity of the demodulated phase is significantly improved, achieving a coefficient of determination (R^2) of 99.9908%, and the method remains robust even when the phase amplitude is as low as $\frac{\pi}{8}$.

These results indicate that the proposed method offers significant advantages in accuracy, stability, and noise resistance, making it highly suitable for high-precision interferometric sensing applications.

Funding. Southern Marine Science and Engineering Guangdong Laboratory (Guangzhou) (SML2023SP231); Hong Kong Research Grants Council (GRF 15209321).

Disclosures. The authors declare no conflicts of interest.

Data availability. Data underlying the results presented in this paper are not publicly available at this time, but may be obtained from the authors upon reasonable request.

References

1. C. Zhou, Y. Pang, L. Qian, *et al.*, "Demodulation of a hydroacoustic sensor array of fiber interferometers based on ultra-weak fiber bragg grating reflectors using a self-referencing signal," J. Lightwave Technol. **37**(11), 2568–2576 (2019).
2. X. Liu, X. Li, S. Li, *et al.*, "A 3 × 3 Phase demodulation system based on active ellipse fitting for 3C fiber-optic geophone array and field tests," J. Lightwave Technol. **42**(14), 5041–5047 (2024).
3. B. G. Gorshkov, A. E. Alekseev, M. A. Taranov, *et al.*, "Low noise distributed acoustic sensor for seismology applications," Appl. Opt. **61**(28), 8308 (2022).
4. W. Lyu, W. Xu, F. Yang, *et al.*, "Non-invasive measurement for cardiac variations using a fiber optic sensor," IEEE Photonics Technol. Lett. **33**(18), 990–993 (2021).
5. W. Lyu, W. Yuan, J. Yu, *et al.*, "Non-contact short-term heart rate variability analysis under paced respiration based on a robust fiber optic sensor system," IEEE Trans. Instrum. Meas. **73**, 1–12 (2024).
6. J. H. López, M. G. Shlyagin, and R. Martínez-Manuel, "Multiplexing and passive demodulation of intrinsic low-finesse Fabry-Perot interferometers using free-running DFB diode lasers," Opt. Laser Technol. **179**, 111346 (2024).
7. X. Zhong, H. Cao, Y. Sun, *et al.*, "Reducing recovery signal distortion of the ϕ-OTDR based on 3×3 coupler demodulation using ellipse fitting algorithm," J. Lightwave Technol. **42**(6), 2200–2208 (2024).
8. Z. Wei, Y. Wu, T. Li, *et al.*, "Cost-effective Φ-OTDR with laser phase noise mitigation using self-mixing interferometry," Opt. Express **33**(5), 11713–11730 (2025).
9. Y.-y. Wang, "Intelligent detection and recognition of multi-vibration events based on distributed acoustic sensor and improved YOLOv8 model," Opt. Fiber Technol. **84**, 103706 (2024).
10. Y. Zhu, Z. Wang, K. Tian, *et al.*, "Phase-generated carrier combined with the Hilbert transform for phase demodulation in frequency-scanning interferometry," Opt. Lasers Eng. **153**, 106988 (2022).
11. L. Yan, Z. Chen, B. Chen, *et al.*, "Precision PGC demodulation for homodyne interferometer modulated with a combined sinusoidal and triangular signal," Opt. Express **26**(4), 4818 (2018).
12. Q. Ge, J. Zhu, G. Zhang, *et al.*, "High stability PGC-EFA-DCM demodulation algorithm integrated with a PID module," J. Lightwave Technol. **40**(24), 7961–7968 (2022).
13. Y. Li, H. Gao, L. Zhao, *et al.*, "Improved PGC demodulation algorithm to eliminate modulation depth and intensity disturbance," Appl. Opt. **61**(19), 5722 (2022).

Optics EXPRESS

14. L. Yan, Y. Zhang, J. Xie, *et al.*, "Nonlinear error compensation of PGC demodulation with the calculation of carrier phase delay and phase modulation depth," J. Lightwave Technol. **39**(8), 2327–2335 (2021).
15. Wang Guo-qing, Xu Tuan-Wei, and Li Fang, "PGC demodulation technique with high stability and low harmonic distortion," IEEE Photonics Technol. Lett. **24**(23), 2093–2096 (2012).
16. Q. Xia, X. Wu, X. Liu, *et al.*, "Low noise 3 × 3 coupler demodulation scheme based on spectral subtraction with multi-window minimum statistical noise estimation," Opt. Express **32**(23), 40416 (2024).
17. X. Liu, X. Wu, J. Luo, *et al.*, "Stably suppressing laser relative intensity noise on a 3 × 3 coupler interferometric system," Opt. Lett. **49**(14), 3950 (2024).
18. S. Pan, Q. Ge, G. Zhang, *et al.*, "High precision 3 × 3 coupler demodulation algorithm with an additional phase shift judgment module," Appl. Opt. **63**(13), 3695 (2024).
19. J. Shi, D. Guang, S. Li, *et al.*, "Phase-shifted demodulation technique with additional modulation based on a 3 × 3 coupler and EFA for the interrogation of fiber-optic interferometric sensors," Opt. Lett. **46**(12), 2900 (2021).
20. H. Hu, Q. Wang, X. Lai, *et al.*, "Integrating polarization diversity into 3 × 3 coupler passive demodulation for interferometric fiber-optic sensors," Opt. Express **33**(7), 16468 (2025).
21. S. Gu, G. Zhang, Q. Ge, *et al.*, "Ameliorated 3 × 3 coupler-based demodulation algorithm using iteratively reweighted ellipse specific fitting," Opt. Express **32**(2), 1108 (2024).
22. Y. Ma, Y. Song, L. Zhang, *et al.*, "A 3×3 Coupler phase demodulation scheme based on three-dimensional ellipsoid fitting," J. Lightwave Technol. **43**, 1–12 (2025).
23. A. Fitzgibbon, M. Pilu, and R. Fisher, "Direct least squares fitting of ellipses," in *Proceedings of 13th International Conference on Pattern Recognition*, vol. 1 (1996), pp. 253–257vol. 1.